

# Multiphoton quantum metrology with neither pre- nor post-selected measurements

Chenglong You,<sup>1</sup> Mingyuan Hong,<sup>1</sup> Peter Bierhorst,<sup>2</sup> Adriana E. Lita,<sup>3</sup> Scott Glancy,<sup>3</sup> Steve Kolthammer,<sup>4</sup> Emanuel Knill,<sup>3,5</sup> Sae Woo Nam,<sup>3</sup> Richard P. Mirin,<sup>3</sup> Omar S. Magaña-Loaiza,<sup>1,\*</sup> and Thomas Gerrits<sup>6</sup>

<sup>1</sup>*Quantum Photonics Laboratory, Department of Physics & Astronomy,  
Louisiana State University, Baton Rouge, LA 70803, USA*

<sup>2</sup>*Mathematics Department, University of New Orleans, New Orleans, Louisiana 70148, USA*

<sup>3</sup>*National Institute of Standards and Technology, 325 Broadway, Boulder Colorado 80305, USA*

<sup>4</sup>*QOLS, Blackett Laboratory, Imperial College London, London SW7 2AZ, United Kingdom*

<sup>5</sup>*Center for Theory of Quantum Matter, University of Colorado, Boulder, Colorado 80309, USA*

<sup>6</sup>*National Institute of Standards and Technology,  
100 Bureau Drive, Gaithersburg, MD 20899, USA*

(Dated: November 10, 2021)

The quantum statistical fluctuations of the electromagnetic field establish a limit, known as the shot-noise limit, on the sensitivity of optical measurements performed with classical technologies. However, quantum technologies are not constrained by this shot-noise limit. In this regard, the possibility of using every photon produced by quantum sources of light to estimate small physical parameters, beyond the shot-noise limit, constitutes one of the main goals of quantum optics. Here, we contribute to this goal by experimentally demonstrating multiphoton quantum-enhanced phase estimation. For the first time, we demonstrate a quantum enhancement in the estimation of a broad range of optical phases with neither pre- nor post-selected measurements. This is achieved through the efficient design of a source of spontaneous parametric down-conversion in combination with photon-number-resolving detection. The robustness of two-mode squeezed vacuum states against loss allows us to outperform schemes based on N00N states, in which the loss of a single photon is enough to remove all phase information from a quantum state. Our work is important for quantum technologies that rely on multiphoton interference such as quantum imaging, boson sampling and quantum networks.

The quantum theory of electromagnetic radiation predicts statistical fluctuations for diverse sources of light [1–4]. Indeed, the underlying amplitude and phase fluctuations of photons establish a quantum limit for the uncertainty of optical measurements made using classical states of light [5]. These fundamental properties of light have enabled scientists to identify the shot-noise limit as the classical limit for precision measurements [6–8]. Remarkably, states of light characterized by nonclassical statistical properties can, in principle, surpass the shot-noise limit [5, 9–16]. This possibility has triggered an enormous interest in the experimental demonstration of quantum-enhanced measurements [17–20]. Unfortunately, efficient and universal schemes for quantum metrology have remained elusive due to stringent technical requirements. Nevertheless, the possibility of estimating small physical parameters with greater sensitivity has important implications for diverse quantum technologies ranging from quantum communication to quantum information processing [21–26].

Over the past three decades, there has been a strong impetus to employ quantum multiphoton states, as well as diverse measurement schemes, to demonstrate estimation of phase shifts with sensitivities that surpass the shot-noise limit [27, 28]. Hitherto, N00N states, an example of multiphoton path-entangled states, have been extensively used to demonstrate super-resolution in quantum metrology [28–34]. Despite the relevance that these quantum states of light have for quantum metrology,

their generation is extremely difficult, particularly when the N00N state involves more than two photons [28]. These challenges have motivated the exploration of conditional schemes that rely on pre- or post-selective measurements [31–39]. In experiments with “pre-selection”, researchers have increased the resolution of phase measurements by conditioning experiments on the observation of specific photon detections that herald the presence of a desired quantum state before the state interacts with the sample to be measured [31, 32, 36]. Conversely, implementations of optical phase estimation based on “post-selection” have been demonstrated by conditioning the outcomes of experiments on specific detection events after the probe state has passed through the sample [33–35, 37–39]. Unfortunately, both protocols discard photons that represent valuable resources for interrogation of phase elements, and in practice pre- and post-selected schemes often succeed with low probability. Thus far, all demonstrations of quantum metrology for phase estimation have relied on either pre- or post-selected measurements or have lacked photon-number resolution [27, 28, 31–39]. Nevertheless, theoretical studies suggest that counting of resources only when pre- or post-selection is successful may lead to enhanced sensitivities beyond the shot-noise limit [40–42].

In 2017, Slussarenko and co-workers demonstrated the first N00N-state based quantum metrology protocol that did not rely on post-selection [27]. That protocol relied on the generation of a high-fidelity N00N state with

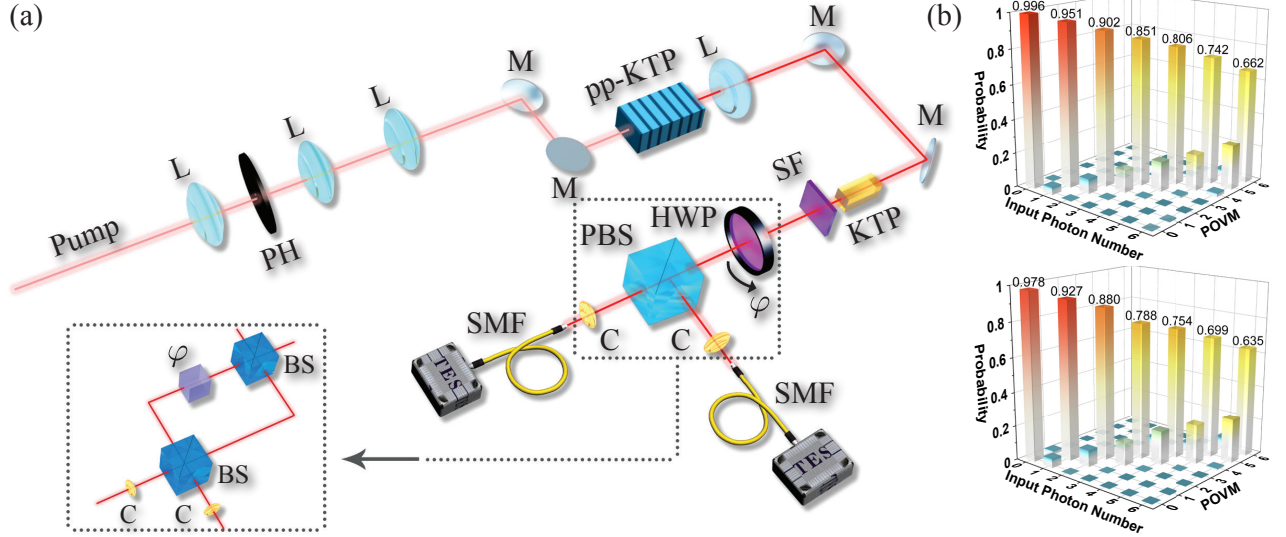


FIG. 1. Experimental setup used to demonstrate multiphoton quantum-enhanced phase estimation. (a) We generate two-mode squeezed vacuum (TMSV) states through a type-II parametric down-conversion process. This is achieved by pumping a periodically poled potassium titanyl phosphate (ppKTP) crystal with a femtosecond Ti:Sapphire laser at 775 nm, cavity dumped with a repetition rate of 76 MHz, which is then pulse-picked at a repetition rate of 229.166 kHz. We use collimation and collection lenses in combination with a  $20\ \mu\text{m}$  pinhole (PH) to filter the spatial profile of the pump beam. The down-converted photons are spectrally filtered by an antireflection-coated piece of silicon (SF) and then injected into a common-path Mach-Zehnder interferometer. Here, two paths of the Mach-Zehnder are replaced with two polarization modes H and V, so that the common-path interferometer implements the same transformation as the traditional Mach-Zehnder interferometer that is shown in the inset. The emerging photons are then coupled into single mode fibers (SMFs) which direct the photons to two transition edge sensors (TESs) with photon number resolution. (b) Quantum detector tomography of our two TESs, we show the reconstructed diagonal positive-operator valued measures (POVMs) for up to 6 photons. L: Lens; M: Mirror; HWP: Half Wave Plate; C: Collimating Lens; BS: Beam Splitter.

$N=2$  photons. Sharing similarities with other schemes that rely on  $N00N$  states, the loss of a single photon in this protocol removes all phase information encoded in the  $N00N$  state [38]. This vulnerability results in higher uncertainties when using  $N00N$  states than when using two-mode squeezed vacuum (TMSV) state for the estimation of optical phase shifts [38, 43, 44]. In addition, higher-order photon generation in spontaneous parametric down-conversion (SPDC) induces errors in protocols that rely on specific photon events to generate perfect  $N00N$  states [27]. Despite the importance of conditional measurements for quantum technologies [45], the possibility of using every photon produced by quantum sources to perform quantum parameter estimation constitutes one of the main goals of quantum optics. Consequently, the first demonstration of multiphoton quantum metrology using photon counting detectors with neither pre- nor post-selected measurements represents an important progression in the field of quantum photonics. Here, we demonstrate a novel scheme that utilizes all the detected photons from a two-mode squeezed vacuum state to perform unconditional quantum-enhanced phase estimation with an overall system efficiency of 80%. This technique relies on an efficient source of SPDC and transition edge sensors that enable the implementation

of photon-number-resolving detection. For the first time, we demonstrate a multiphoton quantum enhancement of 62% in the estimation of the complete range of optical phases.

Our experimental setup is depicted in Fig. 1(a). We use a Ti:Sapphire laser that is spatially filtered by a  $20\ \mu\text{m}$  pinhole and then focused to pump a type-II periodically poled potassium titanyl phosphate (ppKTP) crystal with a length of 2 mm and a poling period of  $46.1\ \mu\text{m}$ . We produce TMSV state with orthogonal polarization H and V at 1550 nm through a process of spontaneous parametric down-conversion. Ideally, the TMSV state is described by  $|z\rangle = \sqrt{1-|z|^2} \sum_{n=0}^{\infty} z^n |n\rangle_s |n\rangle_i$ , where  $n$  denotes the number of photons in the signal (s) and idler (i) modes, and  $z$  represents the squeezing parameter. The parameter  $z$  depends on the nonlinear properties of the crystal, as well as the pump mode and pump power. The filtered signal and idler photons pass through a rotated KTP crystal that compensates for temporal differences between signal and idler photons. Our protocol for phase estimation uses a common-path Mach-Zehnder interferometer (MZI). Here, the two paths of a conventional MZI are replaced with two polarization modes H and V. The phase  $\phi$  that we estimate in our experiment is controlled by a half-wave plate (HWP). Finally, signal

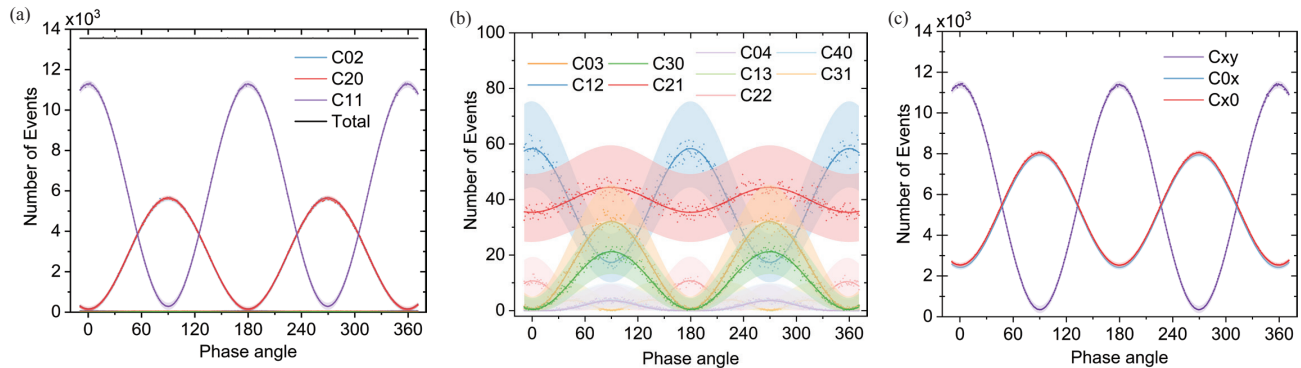


FIG. 2. Experimental measurement of multiphoton interference events in our protocol for quantum metrology. The detection events produced by multiphoton interference are shown in (a) and (b). We use “ $Cmn$ ” to label the detection of  $m$  photons in TES1 and  $n$  photons in TES2. In (a), the C20 data overlaps C02. In (b) we expand the vertical axis to show the higher photon-number detection events, which are not clearly visible at the bottom of (a). Furthermore, in (c) we show how the data of (a) and (b) would have appeared if we used click detectors. Here “ $Cxy$ ” shows events with at least 1 photon detected in both modes, “ $C0x$ ” shows events with no photons detected in signal mode and at least one detected in idler mode, and “ $Cx0$ ” shows events with at least one photon detected in signal mode and no photons detected in idler mode. We use a theoretical model together with our photon-number-resolving measurements to obtain the traces in (c). The data points (dots) in (a) and (b) are generated from averaging nine repeated trials, and each line represents the fit to the nine datasets. All shaded areas correspond to the 95% confidence bounds for the fitted number of events.

and idler photons interfere at a polarizing beam-splitter (PBS). The transmitted and reflected photons are then collected by single-mode fibers, and detected by superconducting transition edge sensors (TESs) with photon-number resolution.

In order to characterize the performance of our experimental setup, we use calibrated superconducting nanowire single photon detectors (SNSPDs). These detectors are used to measure the Hong-Ou-Mandel visibility of  $\mathcal{V} = 99.36(5)\%$  for our common-path interferometer. We also determine the overall detection efficiencies (source to SNSPD) of the system. This in turn allows us to estimate the overall source-to-fiber efficiencies for each of the arms. In our experiment, we implement photon-number-resolving detection with TESs that were characterized through quantum detector tomography [46]. We estimate the efficiencies of our TESs from the tomography data shown in Fig. 1(b). The details of the tomography method can be found in the Supplemental Material. Furthermore, we estimate the overall system detection efficiencies (source to TES) for each of the outputs of our experiment. All the efficiencies are listed in Table I.

TABLE I. Experimental efficiencies of our setup.

Efficiency	Arm1	Arm2
SNSPD	95.9(5)%	92.3(5)%
Overall (SNSPD)	83.42(7)%	79.11(7)%
Source to Fiber	87.0(9)%	85.7(9)%
TES	92.6(1.0)%	95.1(1.0)%
Overall (TES)	80.5(1.2)%	81.5(1.2)%

As shown in Fig. 2(a) and (b), the TESs enable us to probe all the possible multiphoton interference events,

up to 4 photons. The black dotted line in Fig. 2(a) shows that the total number of detected photons does not depend on the phase. We omit the vacuum events and single-photon events in the plot, which are nearly constant for varying phase angles and therefore do not contribute significantly to the ability to detect changes in this parameter (See Supplemental Material). This means that these events do not contribute to the sensitivity of our phase estimation measurements. Moreover, in Fig. 2(b) we plot the traces produced by three- and four-particle interference. The photon-number resolution of our protocol enables the identification of the complex multiparticle interactions that take place in our experiment. Every photon count conveys relevant information regarding the phase that we aim to estimate. This information is not available in quantum metrology protocols that rely on click detectors, which can distinguish zero from one or more photons but otherwise lack photon number resolution. Furthermore, our scheme enables the estimation of a broad range of phases with sensitivities that surpass the shot-noise limit. To compare our results to those that would be obtained without photon number resolving detectors, we reconstruct interference structures obtained with click detectors in Fig. 2(c).

To quantify the performance of our metrology device, we use the classical Fisher information  $\mathcal{F} = \sum_i \left( \frac{\partial \ln p_i}{\partial \phi} \right)^2 p_i$ , where the probability  $p_i$  includes all possible detection results for an experimental trial, i.e.  $i \in \{00, 01, 10, 11, \dots\}$ , so  $\mathcal{F}$  quantifies the information gained in each trial. Each  $p_i$  is estimated using the data given in Fig. 2. Probabilities that do not vary with  $\phi$ , such as the probability  $p_{00}$  of a vacuum event, contribute

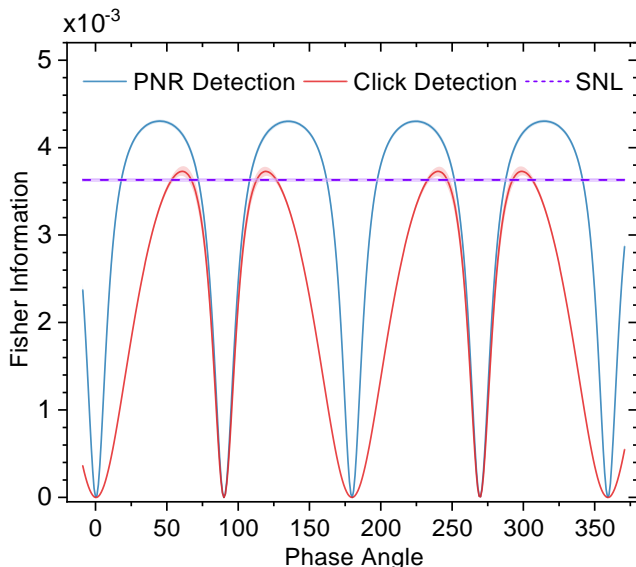


FIG. 3. Experimental Fisher information obtained by using the photon events shown in Fig. 2. The blue (red) line represents the Fisher information of our setup with (without) photon-number-resolving detection. The purple dashed line represents the shot-noise limit (SNL) of our experiment. This limit is established by fitting our experimental data to the theoretical model of our experiment. Here, the SNL is calculated by estimating the number of photons generated through the process of spontaneous parametric down-conversion. The faint shaded areas correspond to the 95% confidence bounds. The 95% confidence bounds for the Fisher information is calculated based on a bootstrapping method using the data shown in Fig. 2. We use the uncertainty of the fitted parameters in the theoretical model of our experiment to calculate the 95% confidence bound for the SNL.

zero for the corresponding term in the sum defining  $\mathcal{F}$ . As shown in Fig. 3, we have calculated the Fisher information, as well as the shot-noise limit given by  $\mathcal{F}_{\text{SNL}} = \bar{n}$ , the average number of photons generated per experimental trial, derived from our experimental results. The average photon number  $\bar{n} = 3.631(14) \times 10^{-3}$ , is estimated by fitting our experimental data to the theoretical model of our setup. Such an approach takes all losses into account, including the mode mismatch at the generation of entangled photons, fiber-coupling loss as well as the loss of our TESs. The details of the calculation can be found in the Supplemental Material. The blue line represents the Fisher information estimated for a detection scheme with photon-number resolution. As a comparison, we plot the Fisher information using the click detector data presented in Fig. 2 (c), which shows lower Fisher information at all angles. Also, the click detector measurement barely reaches the shot-noise limit represented by the purple dashed line, whereas the measurement with TESs surpasses the shot-noise limit for an impressively broad range of 62% of the phase angles. It is worth highlighting the robustness of our protocol against losses. Re-

markably, our scheme for quantum metrology allows for phase estimation with sensitivities that surpass the shot-noise limit, even in dissipative environments with up to 28% loss, meaning that in our specific experimental realization, inserting a sample with up to about 11% loss would still have surpassed the shot-noise limit at a phase angle of  $\phi = \pi/4$ . This prediction is obtained based on our theoretical model outlined in the Supplementary Material. These results demonstrate the superior performance of our metrology scheme utilizing photon-number-resolved detection.

Over the past three decades, scientists and engineers have developed technology and explored novel quantum states of light, as well as quantum measurement schemes, with the aim to demonstrate unconditional quantum protocols. For the first time, we demonstrated the possibility of using photon-number resolution detectors with quantum sources of light to estimate optical phase shifts with sensitivities that surpass the shot-noise limit over a wide range. The broad-peaked Fisher information in our metrology experiment enables one to exceed the shot-noise limit for almost 62% of the phase space even in the presence of losses. This unique feature of our technique is important for quantum-enhanced phase measurement applications such as quantum imaging [47, 48]. Furthermore, our technique is relevant for other quantum technologies that rely on nonclassical multiphoton interference, such as boson sampling and quantum networks [22, 49–51].

## ACKNOWLEDGEMENTS

C.Y. and O.S.M-L. acknowledge funding from the U.S. Department of Energy, Office of Basic Energy Sciences, Division of Materials Sciences and Engineering under Award DE-SC0021069. M. H. thanks the Department of Physics and Astronomy at LSU for funding. T.G., C.Y. and O.S.M-L. thank Animesh Datta, Peter Humphreys, Oliver Slattery and Alan Migdall for helpful discussions. We all acknowledge late Prof. J. P. Dowling for helpful discussions.

## COMPETING INTERESTS

The authors declare that they have no competing interests.

## DATA AVAILABILITY

The data sets generated and/or analyzed during this study are available from the corresponding author or last author on reasonable request.



---

\* maganaloaiza@lsu.edu

- [1] R. J. Glauber, *Phys. Rev.* **130**, 2529 (1963).
- [2] V. V. Dodonov, *J. Opt. B: Quantum Semiclass. Opt.* **4**, R1 (2002).
- [3] C. Gerry and P. Knight, *Introductory Quantum Optics* (Cambridge University Pr., 2004).
- [4] G. S. Agarwal, *Quantum Optics* (Cambridge University Pr., 2012).
- [5] C. M. Caves, *Phys. Rev. D* **23**, 1693 (1981).
- [6] M. Jarzyna and R. Demkowicz-Dobrzański, *Phys. Rev. A* **85**, 011801 (2012).
- [7] M. D. Lang and C. M. Caves, *Phys. Rev. Lett.* **111**, 173601 (2013).
- [8] M. Takeoka, K. P. Seshadreesan, C. You, S. Izumi, and J. P. Dowling, *Phys. Rev. A* **96**, 052118 (2017).
- [9] V. Giovannetti, S. Lloyd, and L. Maccone, *Science* **306**, 1330 (2004).
- [10] V. Giovannetti, S. Lloyd, and L. Maccone, *Nat. Photonics* **5**, 222 (2011).
- [11] R. Krischek, C. Schwemmer, W. Wiecek, H. Weinfurter, P. Hyllus, L. Pezzé, and A. Smerzi, *Phys. Rev. Lett.* **107**, 080504 (2011).
- [12] A. Datta, L. Zhang, N. Thomas-Peter, U. Dorner, B. J. Smith, and I. A. Walmsley, *Phys. Rev. A* **83**, 063836 (2011).
- [13] K. R. Motes, J. P. Olson, E. J. Rabeaux, J. P. Dowling, S. J. Olson, and P. P. Rohde, *Phys. Rev. Lett.* **114**, 170802 (2015).
- [14] R. Demkowicz-Dobrzański, M. Jarzyna, and J. Kołodyński (Elsevier, 2015) pp. 345 – 435.
- [15] C. You, S. Adhikari, X. Ma, M. Sasaki, M. Takeoka, and J. P. Dowling, *Phys. Rev. A* **99**, 042122 (2019).
- [16] M. D. Lang and C. M. Caves, *Phys. Rev. A* **90**, 025802 (2014).
- [17] M. Kacprowicz, R. Demkowicz-Dobrzański, W. Wasilewski, K. Banaszek, and I. A. Walmsley, *Nat. Photonics* **4**, 357 (2010).
- [18] H. Yonezawa *et al.*, *Science* **337**, 1514 (2012).
- [19] M. D. Vidrighin, G. Donati, M. G. Genoni, X.-M. Jin, W. S. Kolthammer, M. S. Kim, A. Datta, M. Barbieri, and I. A. Walmsley, *Nat. Commun.* **5**, 3532 (2014).
- [20] K. Goda, O. Miyakawa, E. E. Mikhailov, S. Saraf, R. Adhikari, K. McKenzie, R. Ward, S. Vass, A. J. Weinstein, and N. Mavalvala, *Nat. Phys.* **4**, 472 (2008).
- [21] V. Giovannetti, S. Lloyd, and L. Maccone, *Phys. Rev. Lett.* **96**, 010401 (2006).
- [22] F. Dell’Anno, S. D. Siena, and F. Illuminati, *Phys. Rep.* **428**, 53 (2006).
- [23] J. Abadie *et al.*, *Nat. Phys.* **7**, 962 (2011).
- [24] O. S. Magaña-Loaiza and R. W. Boyd, *Rep. Prog. Phys.* **82**, 124401 (2019).
- [25] C. You, A. C. Nelliikka, I. D. Leon, and O. S. Magaña-Loaiza, *Nanophotonics* **9**, 1243 (2020).
- [26] C. You, M. A. Quiroz-Juárez, A. Lambert, N. Bhusal, C. Dong, A. Perez-Leija, A. Javaid, R. d. J. León-Montiel, and O. S. Magaña-Loaiza, *Appl. Phys. Rev.* **7**, 021404 (2020).
- [27] S. Slussarenko, M. M. Weston, H. M. Chrzanowski, L. K. Shalm, V. B. Verma, S. W. Nam, and G. J. Pryde, *Nat. Photonics* **11**, 700 (2017).
- [28] E. Polino, M. Valeri, N. Spagnolo, and F. Sciarrino, *AVS Quantum Sci.* **2**, 024703 (2020).
- [29] J. P. Dowling, *Contemp. Phys.* **49**, 125 (2008).
- [30] P. M. Anisimov, G. M. Raterman, A. Chiruvelli, W. N. Plick, S. D. Huver, H. Lee, and J. P. Dowling, *Phys. Rev. Lett.* **104**, 103602 (2010).
- [31] T. Nagata, R. Okamoto, J. L. O’Brien, K. Sasaki, and S. Takeuchi, *Science* **316**, 726 (2007).
- [32] Z.-E. Su, Y. Li, P. P. Rohde, H.-L. Huang, X.-L. Wang, L. Li, N.-L. Liu, J. P. Dowling, C.-Y. Lu, and J.-W. Pan, *Phys. Rev. Lett.* **119**, 080502 (2017).
- [33] P. Walther, J.-W. Pan, M. Aspelmeyer, R. Ursin, S. Gasparoni, and A. Zeilinger, *Nature* **429**, 158 (2004).
- [34] I. Afek, O. Ambar, and Y. Silberberg, *Science* **328**, 879 (2010).
- [35] M. W. Mitchell, J. S. Lundeen, and A. M. Steinberg, *Nature* **429**, 161 (2004).
- [36] G. S. Thekkadath *et al.*, *npj Quantum Inf.* **6**, 89 (2020).
- [37] C. F. Wildfeuer, A. J. Pearlman, J. Chen, J. Fan, A. Migdall, and J. P. Dowling, *Phys. Rev. A* **80**, 043822 (2009).
- [38] N. Thomas-Peter, B. J. Smith, A. Datta, L. Zhang, U. Dorner, and I. A. Walmsley, *Phys. Rev. Lett.* **107**, 113603 (2011).
- [39] J. C. Matthews, X.-Q. Zhou, H. Cable, P. J. Shadbolt, D. J. Saunders, G. A. Durkin, G. J. Pryde, and J. L. O’Brien, *npj Quantum Inf.* **2**, 16023 (2016).
- [40] G. B. Alves, B. M. Escher, R. L. de Matos Filho, N. Zagury, and L. Davidovich, *Phys. Rev. A* **91**, 062107 (2015).
- [41] L. Zhang, A. Datta, and I. A. Walmsley, *Phys. Rev. Lett.* **114**, 210801 (2015).
- [42] D. R. Arvidsson-Shukur, N. Y. Halpern, H. V. Lepage, A. A. Lasek, C. H. Barnes, and S. Lloyd, *Nat. Commun.* **11**, 1 (2020).
- [43] X.-X. Zhang, Y.-X. Yang, and X.-B. Wang, *Phys. Rev. A* **88**, 013838 (2013).
- [44] P. A. Knott, T. J. Proctor, K. Nemoto, J. A. Dunningham, and W. J. Munro, *Phys. Rev. A* **90**, 033846 (2014).
- [45] O. S. Magaña-Loaiza, R. d. J. León-Montiel, A. Perez-Leija, A. B. U’Ren, C. You, K. Busch, A. E. Lita, S. W. Nam, R. P. Mirin, and T. Gerrits, *npj Quantum Inf.* **5**, 80 (2019).
- [46] J. S. Lundeen, A. Feito, H. Coldenstrodt-Ronge, K. L. Pregnell, C. Silberhorn, T. C. Ralph, J. Eisert, M. B. Plenio, and I. A. Walmsley, *Nat. Phys.* **5**, 27 (2009).
- [47] L. A. Lugiato, A. Gatti, and E. Brambilla, *J. Opt. B: Quantum Semiclass. Opt.* **4**, S176 (2002).
- [48] G. Brida, M. Genovese, and I. Ruo Berchera, *Nat. Photonics* **4**, 227 (2010).
- [49] M. Tillmann, B. Dakić, R. Heilmann, S. Nolte, A. Szameit, and P. Walther, *Nat. Photonics* **7**, 540 (2013).
- [50] H. Wang *et al.*, *Nat. Photonics* **11**, 361 (2017).
- [51] J. B. Spring *et al.*, *Science* **339**, 798 (2013).
- [52] A. E. Lita, A. J. Miller, and S. W. Nam, *Opt. Express* **16**, 3032 (2008).

## SUPPLEMENTAL MATERIAL

### Detectors tomography

We characterize our TESs by performing quantum detector tomography. The purpose of this technique is to characterize the TES response given a photon number state in the input. In this context, the detector response is described by the detector's positive-operator valued measure (POVM). Since it is not possible to generate arbitrary Fock states on demand, we use varying weak coherent states and employ a tomographic reconstruction of the POVMs [46]. For both TESs, we assume no phase dependence; therefore the POVM elements are diagonal in the Fock basis. The POVM element corresponding to detecting  $n$  photons is  $\{\pi_n\}$ , and the  $k^{\text{th}}$  diagonal entry of  $\pi_n$  is  $\pi_n(k) = \theta_k^{(n)} |k\rangle\langle k|$ , where  $|k\rangle$  is the  $k$ -photon Fock vector. We probe the TESs with a set of  $m$  coherent-state probes with different amplitudes  $\alpha_m$ . A coherent state with amplitude  $\alpha_m$  has probability  $C_{m,k} = |\alpha_m|^{2k} \exp(-|\alpha_m|^2) / k!$  to contain  $k$  photons. Here the Hilbert space needs to be truncated at some finite photon number, and for our purpose we choose to truncate at  $k = 9$ . By constructing the POVM set matrix  $\Pi$  as  $\Pi_{k,n} = \theta_k^{(n)}$ , we can write the measured statistics matrix  $R$  as a matrix equation  $R = C\Pi$ . Therefore, the matrix element  $R_{m,n}$  represents the probability to observe  $n$  photons when a coherent state with amplitude  $\alpha_m$  is given. Finally, since we have a calibrated set of coherent probe states encoded in  $C$  and the estimates of measurement probabilities in  $R$ , we can use maximum likelihood to estimate  $\Pi$ , which encodes the POVMs for the TESs. The corresponding results are plotted in Fig. 1 (b).

### Resource counting

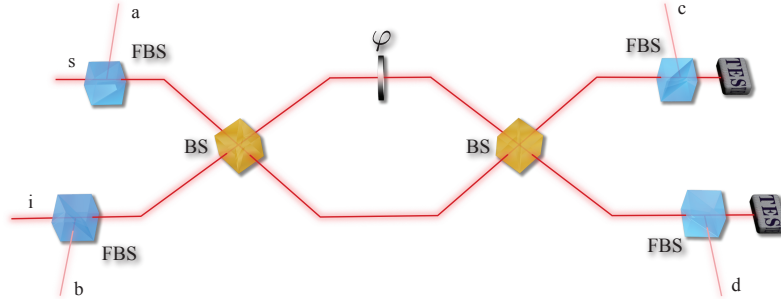


FIG. 4. The theoretical model of our experimental setup when considering loss. We model the loss of the state preparation and the loss of the setup as well as fiber coupling, using several fictitious beam splitters (FBSs). In addition, we model the loss of the detector using the detector tomography data as shown in Fig. 1(b), rather than the estimated detector efficiency.

The quantum enhancement of our metrology setup is justified by comparing the classical Fisher information of the measurement outcome with the shot-noise limit (SNL). In terms of the Fisher information, the SNL is given by  $\mathcal{F}_{\text{SNL}} = \bar{n}$ . To estimate  $\mathcal{F}_{\text{SNL}}$ , we need to accurately count the number of photons generated by the ppKTP crystal. Our common-path Mach-Zehnder interferometer can be represented schematically as a regular Mach-Zehnder interferometer as in Fig. 4. The ppKTP crystal generates a two-mode squeezed vacuum state

$$|\psi\rangle_1 = \sqrt{1 - |z|^2} \sum_{n=0}^{\infty} z^n |n\rangle_s |n\rangle_i, \quad (1)$$

with  $\hat{\sigma}_1 = |\psi\rangle_1 \langle \psi|$ . Under realistic conditions, our model has to consider the imperfect state generation, lossy optical elements as well as the non-unity probability of free space to fiber coupling. We model these losses by adding fictitious beam splitters into the optical paths. Using the notation of  $\hat{X} \circ \hat{Y} \equiv \hat{X} \hat{Y} \hat{X}^\dagger$ , the generated two-mode squeezed vacuum

state  $\hat{\sigma}_1$  would evolve under

$$\hat{\sigma}_2 = \text{Tr}_{ab} \left[ \hat{U}_{as}^{\text{BS}}(\eta_p) \circ \hat{U}_{bi}^{\text{BS}}(\eta_p) \circ \left( \hat{\sigma}_1 \otimes \hat{\vartheta}_a \otimes \hat{\vartheta}_b \right) \right], \quad (2)$$

$$\hat{\sigma}_3 = \hat{U}_{si}^{\text{BS}}(1/2) \circ \left( \hat{P}_s(\theta) \otimes \hat{P}_s(0) \right) \circ \hat{U}_{si}^{\text{BS}}(1/2) \circ \hat{\sigma}_2, \quad (3)$$

$$\hat{\sigma}_4 = \text{Tr}_{cd} \left[ \hat{U}_{cs}^{\text{BS}}(\eta_d) \circ \hat{U}_{di}^{\text{BS}}(\eta_d) \circ \left( \hat{\sigma}_1 \otimes \hat{\vartheta}_c \otimes \hat{\vartheta}_d \right) \right]. \quad (4)$$

Here  $\vartheta$  is a vacuum mode,  $\hat{U}_{as}^{\text{BS}}$  is the beam splitter unitary operator between mode  $a$  and mode  $s$  and  $\hat{P}_s(\theta)$  is the phase shift operator on mode  $s$ . And finally, the probability of detecting  $j$  and  $k$  photons in modes  $s$  and  $i$  is then given by

$$p(j, k) = \sum_{m, n} \text{Tr} \left[ \hat{\sigma}_4 \pi_m^s(j) \pi_n^i(k) \right], \quad (5)$$

where  $\pi_m^s$  and  $\pi_n^i$  are the POVM elements of the TESs. To estimate the average number of photons generated at the ppKTP crystal, we numerically evaluate and fit our experimental data to these equations above. Therefore, we can determine the average number of photons generated at the ppKTP crystal, using  $\bar{n} = |z|^2 / (1 - |z|^2)$ . Note that due to loss during and after photon generation,  $\bar{n}$  is an overestimate of the number of photons that enter the HWP that determines  $\phi$ , so if that number was the relevant metrological resource,  $\mathcal{F}_{\text{SNL}}$  would be an overestimate of the shot-noise limit. However, since our setup is a common-path interferometer, and the spectral filter (SF) and the KTP crystal are low loss, we assume that the number of photons that pass through the HWP is close to  $\bar{n}$ .

It is worth highlighting the robustness of our protocol against losses. Our scheme for quantum metrology allows for phase estimation with sensitivities that surpass the shot-noise limit, even in dissipative environments characterized by 28% loss. This prediction is obtained based on our theoretical model, by increasing losses represented by the fictitious beam splitters in each optical path.

### Single-photon events

Fig. 5 shows experimental multiphoton interference, which includes single-photon events. As discussed in the main text of our manuscript, due to the slightly imbalanced efficiencies of our setup, the probabilities of these single-photon events slightly vary with respect to the angle of the phase shifter. These events contribute to the Fisher information four orders of magnitude less than other terms. However, as shown in Fig. 5, the frequency of single-photon events C01 and C10 is larger than that of multiphoton events. These single-photon events are produced by two processes; photons generated by SPDC in our experiment and black-body radiation. The energy of black-body photons is similar to that of our SPDC photons. Consequently, due to the broad wavelength sensitivity and the limited energy resolution of our TESs [52], the TES signal induced by black-body photons may overlap with the signal produced by SPDC photons, leading to a ‘false’ single-photon event. This undesirable effect is negligible for two-photon coincidence events C11. Indeed, a two-photon event produced by black-body radiation is unlikely. Thus, the contamination of black-body photons dominates single-photon events C10 and C01. This is due to the high efficiency of our setup and the low pair generation probability of our SPDC source. Furthermore, we note that the magnitude of the contamination differs with respect to the detectors. We emphasize that shot-noise limit analysis presented in the body of the manuscript does not include contributions from black-body photons, since these black-body photons do not interact with the varying phase in the setup.

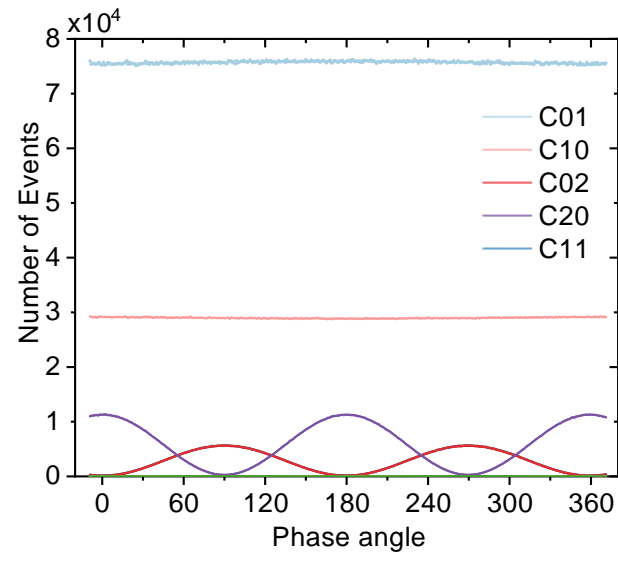


FIG. 5. Experimental measurement of multiphoton interference events in our protocol.